Microemulsion-made Gadolinium Carbonate Hollow Nanospheres Showing Magnetothermal Heating and Drug Release

J. Jung-König,[a] M. Sanhaji,[b] R. Popescu,[c] C. Seidl,[d] E. Zittel,[d] U. Schepers,[d,e] D. Gerthsen,[c] I. Hilger,[b] and C. Feldmann[a]*

[a]Institut für Anorganische Chemie, Karlsruhe Institute of Technology (KIT), Engesserstraße 15, Karlsruhe, 76131, Germany

[b]Institute of Diagnostic and Interventional Radiology, University Hospital Jena, Research Center Lobeda, Am Klinikum 1, 07747 Jena, Germany

[c]Laboratorium für Elektronenmikroskopie, Karlsruhe Institute of Technology (KIT), Engesserstraße 7, 76131 Karlsruhe, Germany

[d]Institute of Toxicology and Genetics, Karlsruhe Institute of Technology (KIT), Hermann-von-Helmholtz-Platz 1, 76344 Eggenstein-Leopoldshafen, Germany

[e]Institute of Organic Chemistry, Karlsruhe Institute of Technology (KIT), Fritz Haber Weg 6, 76131 Karlsruhe, Germany

SUPPORTING INFORMATION

Content

1. Analytical techniques

Fourier-transform infrared (FT-IR) spectroscopy. Fourier-transform infrared (FT-IR) spectra were recorded using a Bruker Vertex 70 FT-IR spectrometer in the area from 4000 to 370 cm^{-1} with a resolution of 4 cm^{-1} using KBr pellets. To prepare these pellets, 500 mg KBR was mixed with 3 mg of the sample.

X-ray powder diffraction (XRD). XRD measurements were carried out on a θ/2θ Stoe Stadi-P diffractometer by using Cu-$K_{\alpha 1}$ radiation ($\lambda = 1.540598$ Å) monochromated by a focusing germanium crystal. A position-sensitive detector was used for recording the XRD patterns with a step size of 0.03 °(2θ). The detector channels were calibrated with the line positions of a Si standard. The powder samples were prepared in a 0.5 mm capillary.

Differential thermal analysis/thermogravimetry (DTA/TG). DTA/TG was performed with a STA409C device (Netzsch). The measurements were performed under nitrogen. The vacuum dried samples (15 mg in corundum crucibles) were heated to 1000 °C with a heating rate of 10 K/min. TG/IR coupling was performed with the above equipment coupled with a Bruker TGA/IR 588.

Optical spectroscopy (UV-Vis). UV-VIS spectra were recorded using a Varian Cary Scan 100 by measuring diffuse reflection of powder samples with an integrating sphere. $BaSO_4$ was used as a reference.

Photoluminescence spectroscopy. PL spectra were recorded with a Jobin Yvon Spex Fluorolog 3 equipped with a 450 W Xe-lamp and double grating excitation and emission monochromator.

Electron diffraction. HRTEM images were evaluated by calculating the two-dimensional Fourier transform, denoted as diffractogram, which yields information on the crystal structure (lattice parameters and crystal symmetry) of single nanoparticles. The analysis was performed by comparing the experimental diffractograms and the calculated diffraction patterns, where the latter were obtained by using the JEMS (Java version of the electron microscopy simulation) software.[19] The zero-order beam (ZB) is indicated on the diffractograms by a white circle.

2. Structural analysis of the $Gd_2(CO_3)_3$ nanoparticles

The size, structure and chemical composition of the as-prepared $Gd_2(CO_3)_3$ hollow nanospheres was studied based on HRTEM, HAADF-STEM and EDXS (Figures S1,S2; *see main paper: Figure 2*). Histograms obtained from the statistical evaluation of >360 hollow nanospheres, furthermore, allow determine their outer (*D*) and inner diameter (*d*) to $D = 26\pm4$ nm and $d = 7\pm2$ nm (Figure S2a,b). Moreover, the presence of an inner cavity is supported by the integrated intensities of the Gd-*L* series and O-K_{a1} line shown after background subtraction (*Figure S1*; *see main paper: Figure 2c*). The Gd- and O-intensity profiles show a specific intensity dip in the particle center, which is characteristic for the hollow sphere morphology (Figure S1b; *see main paper: Figure 2c*).

In contrast to the intensity profiles, the concentration profiles show a constant ratio of Gd and O all over the hollow nanosphere (*Figure S1c*). This finding confirms the uniform composition of the sphere wall. Since EDXS is less significant for low-weight elements such as oxygen, as well as, due to the drastically different mass of oxygen and gadolinium the observed Gd:O ratio is not indicative in terms of the exact stoichiometry of the compound. Nevertheless, despite of that, the constant Gd:O ratio remains a relevant information. EDXS area scans also reveal the characteristic X-ray lines of the Gd-*L* series and the O-K_{a1} line (Figure S2c,d; *see main paper: Figure 2d,e*). Additional lines (i.e. Cu-*K*, Cu-*L*, C-*K*) are not significant and stem from copper grid and the amorphous carbon substrate. Therefore, the C content of the nanoparticles cannot be quantitatively analyzed via EDXS with sufficient accuracy.

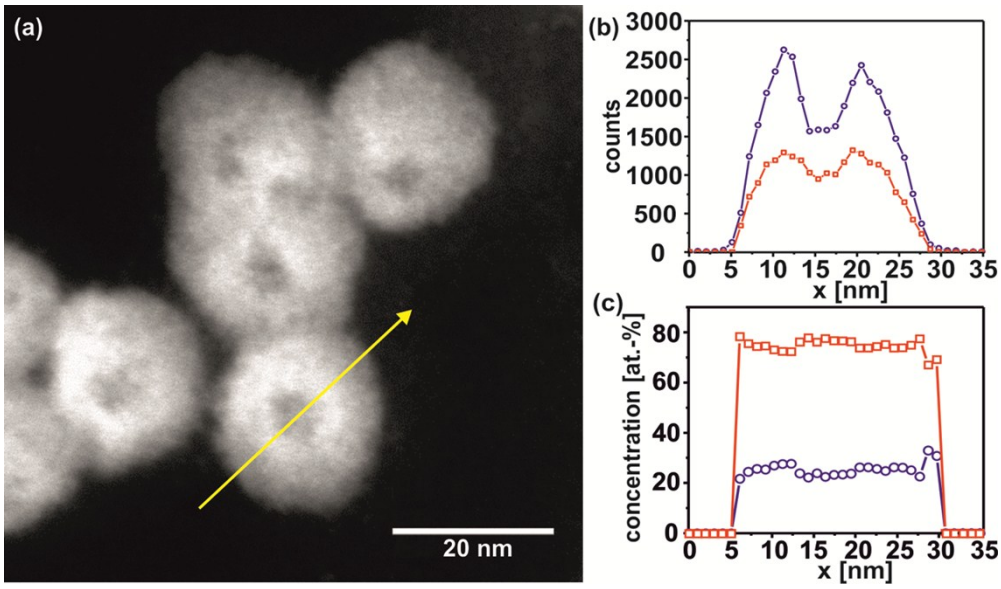

Figure S1. a) HAADF-STEM image of $Gd_2(CO_3)_3$ hollow nanospheres; b) integrated intensities of the Gd-*L* series (blue) and O-K_{a1} line (red) and c) Gd (blue) and O composition (red) profiles measured along the EDXS line scan shown by the arrow in (a).

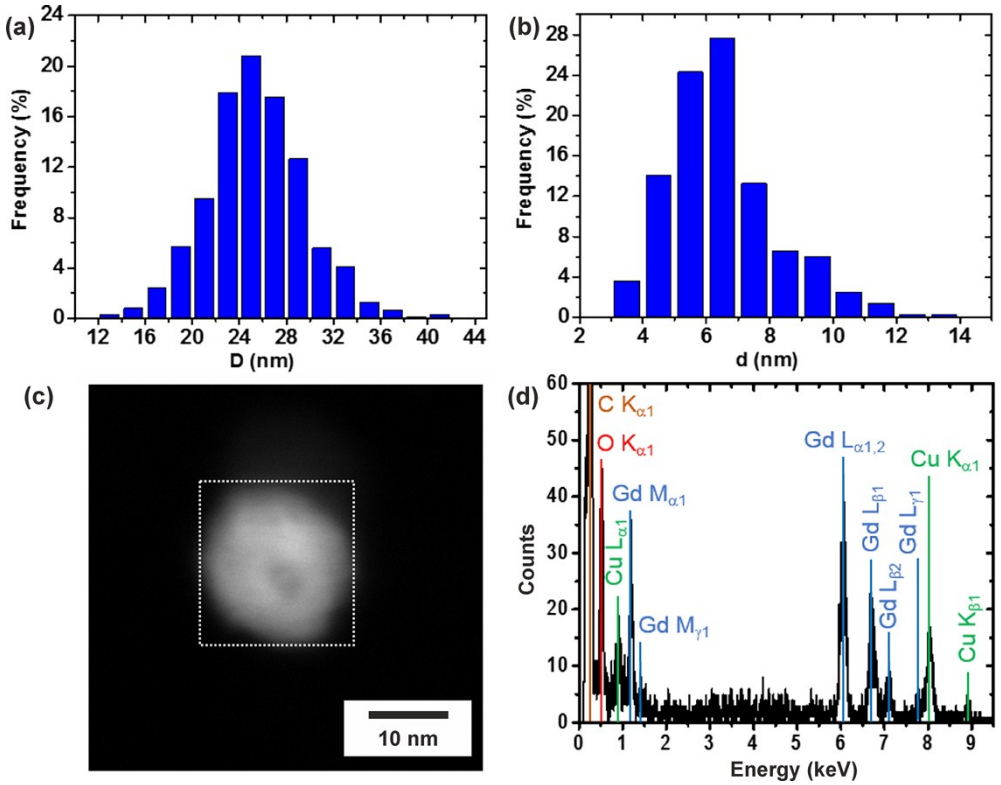

Figure S2. a) Histogram of outer hollow sphere diameters (*D*) and b) histogram of inner cavity diameters (*d*) from >360 hollow nanospheres; c) HAADF-STEM image of a single $Gd_2(CO_3)_3$ hollow nanosphere with the frame indicating an EDXS area scan; d) EDX spectrum from area scan recorded in the frame on (c).

Thermogravimetry (TG) with coupling to Fourier-Transform infrared spectroscopy (FT-IR) showed the release of three equivalents CO_2 per formula unit, which matches with the chemical composition $Gd_2(CO_3)_3$ (*see main paper: Figure 3*). FT-IR coupling proves CO_2 as the dominant decomposition product. Thus, the ν(C=O) vibration (2400-2300 cm^{-1}) has the highest intensity over the complete temperature range (50-1000 °C) (Figure S3). Additional vibrations at lower temperatures (50-400 °C) indicate the release of water from the inner hollow sphere cavity (ν(O–H): 4000-3500 cm^{-1}, δ(O–H): 1750-1300 cm^{-1}) (Figure S3). The thermal remnant after heating to 1000 °C was analyzed by X-ray powder diffraction and turned out as Gd_2O_3 (Figure S4).

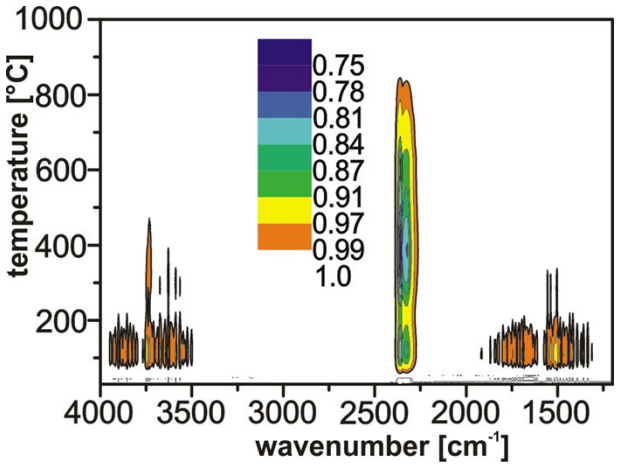

Figure S3. 3-Dimensional diagram of TG with FT-IR coupling showing the temperature dependent release of CO_2 (i.e., ν(C=O) vibration at 2400-2300 cm^{-1}) and H_2O (i.e., vibrations ν(O–H) and δ(O–H) at 4000-3500 and 1750-1300 cm^{-1})) with the intensity of the respective FT-IR absorption.

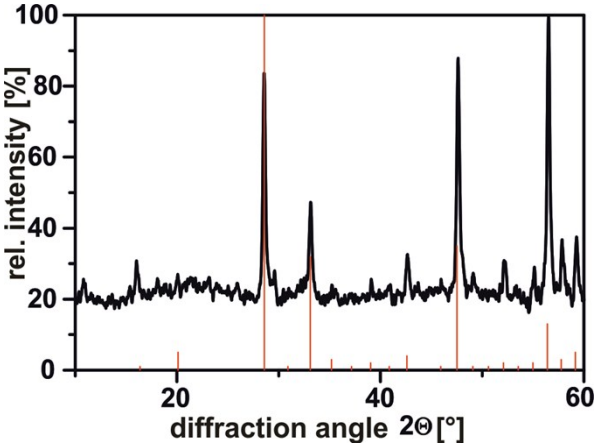

Figure S4. XRD pattern of the TG remnant (red lines: Gd_2O_3 as a reference [1]).

As already discussed in the main paper, the as-prepared $Gd_2(CO_3)_3$ hollow nanospheres start to decompose in the electron microscope after few seconds (5-10 s) under the bombardment with high-energy electrons. Thus, the hollow-sphere structure starts to collapse with destruction of the sphere wall and a formation of solid, crystalline nanoparticles. Using HRTEM, the resulting crystalline solid nanoparticles that were formed after electron-beam irradiation and CO_2 release were identified as $Gd_2O_2(CO_3)$ (Figure S5a). Thus, crystalline domains with mean sizes of about 4 nm, which show continuous lattice fringes can be observed on the HRTEM image in Figure S5a. The two-dimensional Fourier transform of these single-crystalline domains (Figure S5a, inset) shows good agreement with the calculated diffraction pattern of bulk hexagonal-close-packed $Gd_2O_2(CO_3)$ (space group $P6_3/mmc$, $a = 3.9222$, $c = 15.4624$ Å) along the [421] zone axis (Figure S5b). This finding is well in agreement with thermogravimetry (*see main paper: Figure 3*) showing the successive loss of altogether three equivalents of CO_2 according to the following sequence of reactions:

$$Gd_2(CO_3)_3 \rightarrow Gd_2O(CO_3)_2 + CO_2\uparrow \rightarrow Gd_2O_2(CO_3) + CO_2\uparrow \rightarrow Gd_2O_3 + CO_2\uparrow$$

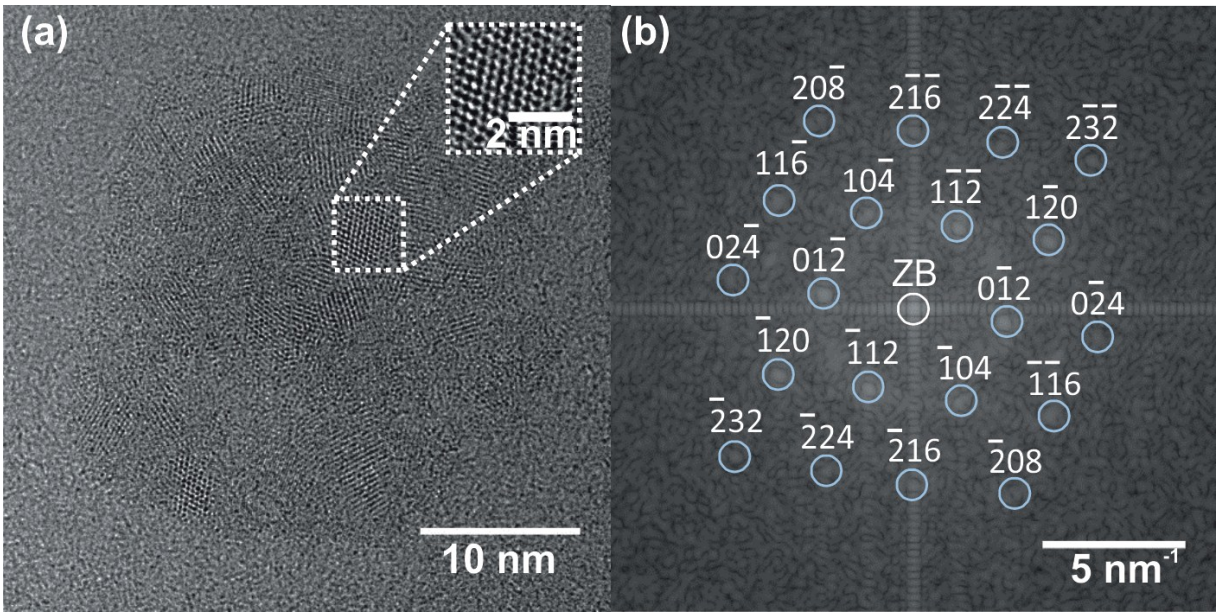

Figure S5. Decomposition and crystallization of the $Gd_2(CO_3)_3$ hollow nanospheres under the electron beam: a) HRTEM image of a single nanoparticle after 5 s illumination at 300 kV showing the formation of crystalline domains; b) Comparison of the two-dimensional Fourier transform of a single-crystalline domain (inset in (a)) and calculated diffraction pattern of bulk-hcp-$Gd_2O_2(CO_3)$ in the [421] zone axis (Bragg reflections are indicated by blue circles, zero-order beam by a white circle).

3. Determination of DOX concentration in DOX@$Gd_2(CO_3)_3$ nanocontainers

Fluorescence spectroscopy of DOX@$Gd_2(CO_3)_3$ nanocontainers shows the expected fluorescence of DOX (Figure S6). Thus, broad excitation in the 300 to 600 nanometer region is observed as well as deep red to infrared emission (550 to 800 nm).

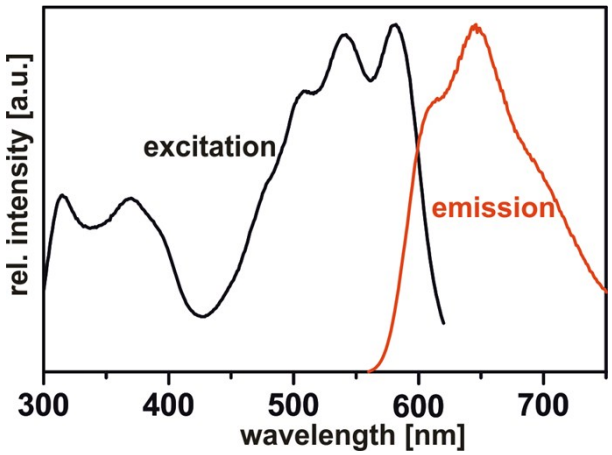

Figure S6. Excitation and emission spectra of DOX@$Gd_2(CO_3)_3$ nanocontainers (emission spectrum recorded at 550 nm excitation).

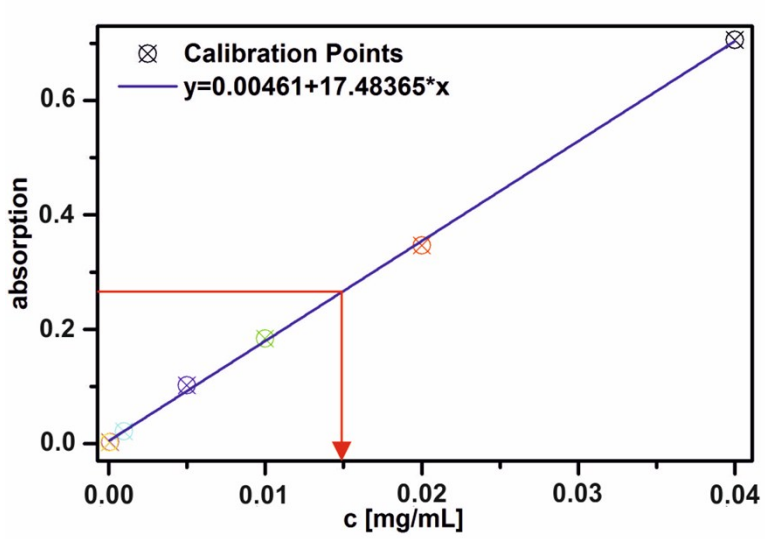

Figure S7. Calibration curve of DOX solutions as references to determine the DOX concentration in the as-prepared DOX@$Gd_2(CO_3)_3$ nanocontainers (determination of the DOX absorption via UV-Vis spectroscopy).

To determine the DOX concentration in the DOX@$Gd_2(CO_3)_3$ nanocontainers the visible absorption was compared to DOX solutions with known DOX concentration as references. To this concern, an aliquot of the DOX@$Gd_2(CO_3)_3$ nanocontainers was centrifuged and

dissolved in 1 mL of a citrate buffer solution at pH 4.7. After 2 h, the $Gd_2(CO_3)_3$ nanocontainers were completely dissolved and the DOX released. The absorption of the resulting solution was measured via UV-Vis spectroscopy. This absorption was compared according to the Lambert-Beer law with a calibrated reference curve (Figure S7). This calibration curve was determined for DOX solutions with DOX concentrations of 0 to 0.04 mg/mL (in citrate buffer at pH 4.7). As a result, the DOX concentration of the DOX@$Gd_2(CO_3)_3$ nanocontainers was determined to 0.0035 mg/mL.

4. In vitro studies (HepG2 cells)

The intracellular distribution and biocompatibility of dextran-coated DOX@$Gd_2(CO_3)_3$ nanocontainers was evaluated by means of confocal laser scanning microscopy (CLSM). Therefore, HeLa cells (*see main paper: Figure 5*) and HepG2 cells (Figure S8) were exposed to DOX@$Gd_2(CO_3)_3$ for 4, 8, 24 and 48 hours during cultivation (0.5 µM DOX). In both cases, DOX@$Gd_2(CO_3)_3$ did not harm the cells immediately, although the uptake and the accumulation in perinuclear regions – as indicated by intense red fluorescence – can already be observed after 4 hours. The fluorescence intensifies at 8 hours and is supplemented by a nuclear uptake of doxorubicin, which causes HeLa cells as well as HepG2 cells after long time exposure to swell entirely and to undergo necrosis (*see main paper: Figure 5*; Figure S8).

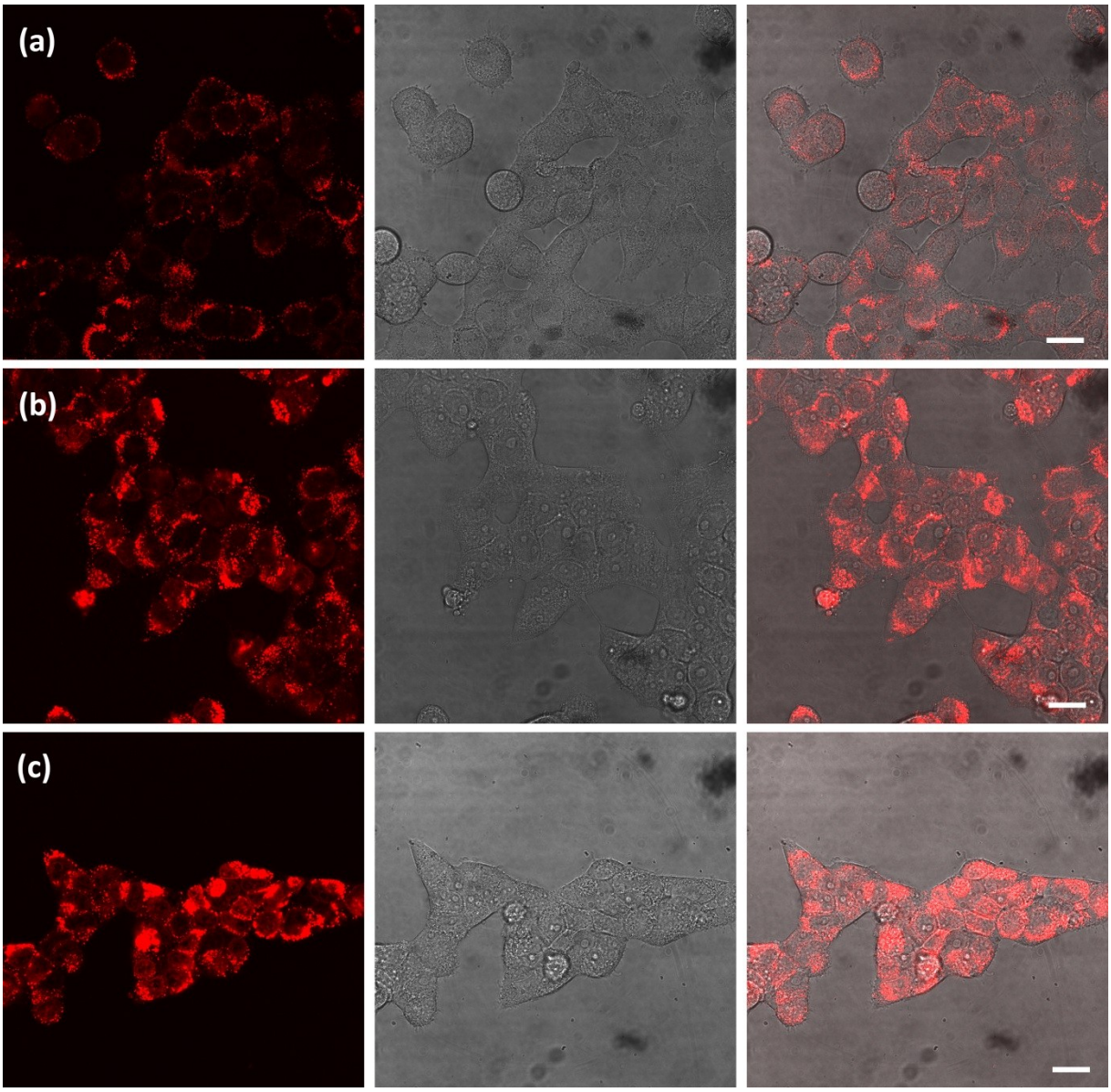

Figure S8. Intracellular distribution of DOX@$Gd_2(CO_3)_3$ in HepG2 cells after 24 hours at different DOX concentrations: a) 0.25, b) 0.5, and c) 1.0 μM. Perinuclear staining indicates endocytotic uptake of the hollow nanospheres (scale bar: 25 μm).

References

1 A. Bartos, K. P. Lieb and M. Uhrmacher, D. Wiarda, *Acta Crystallogr. B,* 1993, **49**, 165.